Development of mantle seismic anisotropy during subduction-induced 3-D flow

M. Faccenda[1,2] and F. A. Capitanio[1]

Received 10 April 2012; revised 5 May 2012; accepted 8 May 2012; published 6 June 2012.

[1] The dynamics of subduction can be indirectly constrained by studying the induced mantle flow. However, inferring the circulation of the mantle around subducting plates from the interpretation of shear wave splitting patterns remains elusive. We calculated the strain-induced lattice preferred orientation (LPO) developed in 3-D models of subduction where retreat motions are maximized and found that in the mantle layer entrained with the downgoing slab the seismic anisotropy is trench-perpendicular, and becomes trench-parallel deeper, where the toroidal flow accommodates slab retreat. Synthetic SKS splitting shows that in the fore-arc slab rollback favors trench-parallel polarization of the fast shear wave component, while plate advance enhances trench-perpendicular seismic anisotropy. The interference between these two competing mechanisms yields subslab delay times of 0.5 to 1.3 sec, comparable with those observed at most natural subduction zones. The magnitude of the subslab trench-parallel splitting is independent of the rate at which the slab migrates, instead it is proportional to the amount of retreat.
Citation: Faccenda, M., and F. A. Capitanio (2012), Development of mantle seismic anisotropy during subduction-induced 3-D flow, *Geophys. Res. Lett.*, *39*, L11305, doi:10.1029/2012GL051988.

1. Introduction

[2] The dynamics of sinking lithosphere and induced mantle flow has a first order control on the thermal and chemical evolution of the upper part of the Earth's mantle. Understanding the 3D nature of mantle flow can indirectly provide useful insights into the dynamics of subduction. Yet, constraining the patterns of mantle circulation around subducting slabs has proven difficult. Shear wave splitting measurements (SWS) provide indirect information on the mantle flow. When a shear wave travels through an anisotropic medium, it splits in two orthogonally polarized components, with the fastest along the plane with the highest seismic velocity. Because anisotropic mantle minerals acquire a lattice preferred orientation (LPO) under strain [*McKenzie*, 1979; *Ribe*, 1992; *Zhang and Karato*, 1995; *Bystricky et al.*, 2000], SWS is commonly interpreted as evidence of mantle deformation during flow [*Savage*, 1999; *Park and Levin*, 2002]. SWS is defined by two parameters: the delay time δt between the arrival of the fast and slow wave components and the azimuth ϕ of the fast wave component. Vertically traveling, long-period SKS waves, generated by the conversion of P waves at the core–mantle boundary, are often used to determine anisotropy. Because diffusion creep is the dominant deformation mechanism in the lower part of the mantle [*Karato et al.*, 1995] and the minerals of the transition zone are weakly anisotropic [*Tommasi et al.*, 2004], the interpretation of the SKS splitting allows inferences on the structure of the upper mantle. However, as SKS waves sample the entire upper mantle, it is difficult to determine the distribution and nature of the mantle anisotropy sources. At subduction zones this problem may be partially overcome by using local or source-side S waves that allow to discriminate between supraslab and subslab anisotropic sources, respectively [e.g., *Di Leo et al.*, 2012].

[3] SKS splitting patterns observed at subduction zones have the following characteristics: ϕ is generally oriented parallel to the trench in the fore-arc and the subslab δt varies from 0.5 to 2–2.5 sec, possibly scaling linearly with the trench migration velocity ($|V_t|$) [*Russo and Silver*, 1994; *Long and Silver*, 2008]. SWS measured with source-side shear waves locate a strong source of anisotropy in the mantle below the subducting slab, beneath the fore-arc [*Müller et al.*, 2008; *Foley and Long*, 2011; *Di Leo et al.*, 2012]. Because ϕ is routinely interpreted by seismologists as indicating the direction of mantle flow, subslab trench-parallel mantle flow with a magnitude proportional to $|V_t|$ has been proposed to explain such observations [*Russo and Silver*, 1994; *Long and Silver*, 2008]. In laboratory models of plate subduction and induced flow, *Buttles and Olson* [1998] used whiskers as an analogue for the olivine a-axis and found that those below a retreating slab tend to align parallel to the trench, whereas the mantle flow is trench-perpendicular there [*Kincaid and Griffiths*, 2003; *Funiciello et al.*, 2006; *Piromallo et al.*, 2006]. This apparent discrepancy agrees well with the analytical solutions obtained by [*Kaminski and Ribe*, 2002], demonstrating that the LPO rarely orients with the flow, except during simple shear deformation. Thus, the interpretation of ϕ as indicating the direction of mantle flow might not always be warranted.

2. Modeling

[4] In order to quantitatively establish the surface expression of the subduction-induced mantle flow and compare it with observations, we quantify the seismic anisotropy due to crystal LPO in 3-D numerical subduction models and estimate synthetic SKS splitting. The subduction of an oceanic lithosphere in a non-Newtonian mantle is modeled in 3-D with Underworld [*Moresi et al.*, 2007] (Figure S1 of Text S1 in the auxiliary material).[1] For each timestep we compute the

[1]School of Geosciences, Monash University, Clayton, Victoria, Australia.
[2]Now at Department of Geoscience, University of Padua, Padua, Italy.

Corresponding author: M. Faccenda, Department of Geoscience, University of Padua, I-35131 Padua, Italy. (manuele.faccenda@gmail.com)

[1]Auxiliary materials are available in the HTML. doi:10.1029/2012GL051988.

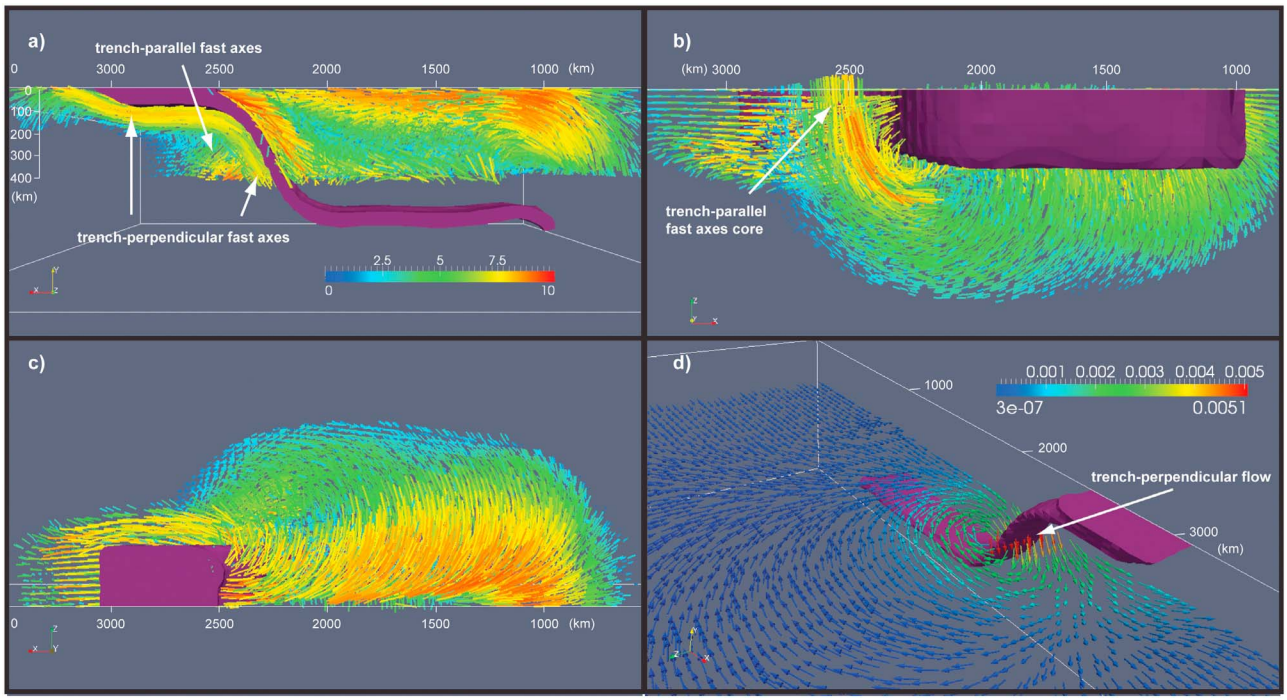

Figure 1. Different views of the dynamic model in Figure S2 of Text S1; t = 17.8 Myr. Only half of the model space is shown, cut on the vertical symmetry midplane. The purple surface is the contour of the density field around the plate. Seismic anisotropy is visualized only in panels (a), (b) and (c). The bars represent the orientation of the symmetry axis of the hexagonal symmetry class calculated with D-Rex. The length and color of each axis is proportional to the amount of anisotropy. The axes indicate fast seismic directions because they are sub-parallel to the maximum stretching directions. (a) Midplane. (b) Bottom; there is a strong trench-parallel anisotropic core below the slab. (c) Top. (d) Velocity field at 300 km depth. The white lines highlight domain boundaries.

development of strain-induced LPO of olivine and enstatite dry aggregates in the mantle, from an initial random distribution, with a version of D-Rex [*Kaminski et al.*, 2004] modified to account for forward advection of particles and 3-D flow. SKS splitting patterns are successively predicted for stations located above the model domain by means of computing seismograms synthetics [*Becker et al.*, 2006] (see auxiliary material for more details about the subduction, LPO and SKS splitting modeling). This workflow allows direct determination of the location and strength of potential mantle anisotropy sources yielding estimates of δt and ϕ at the surface.

3. Results

[5] In the 3D dynamic models the negative buoyancy of the subducting plate drives consistent subduction motions and mantle flow. After sinking through the mantle, the slab reaches the transition zone, followed by plate advance and slab retreat until total consumption of the plate is achieved (Figure S2 of Text S1). A ~100 km thick mantle layer is entrained at depth by the subducting plate and follows the motions of the plate towards the trench. Toroidal flow from the subslab region to the mantle wedge accommodates the retreat of the slab (Figure 1d).

[6] Calculations of seismic anisotropy show that as the oceanic plate subducts, the amount of anisotropy increases progressively, especially in the subslab mantle where two distinct domains are found (Figures 1a, 1b, and S2): the upper is ~100 km thick with a trench-perpendicular anisotropy up to 8% due to the entrained, poloidal mantle flow beneath the slab and is characterized by simple shear deformation (Figure S3 of Text S1). The lower domain extends from the base of the upper domain down to 410 km depth and develops sub-horizontal, trench-parallel orientation of the fast symmetry axis due to pure shear deformation induced by the slab rollback (Figure S3 of Text S1). Retreat of the slab produces a trench-normal compression, causing trench-parallel alignment of the finite strain major axis [*Buttles and Olson*, 1998]. In this deeper domain a strongly anisotropic

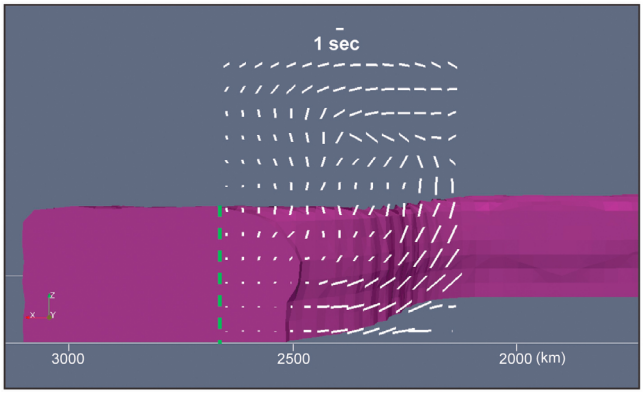

Figure 2. SKS splitting patterns of the dynamic model in Figures 1 and S2; t = 17.8 Myr. The green line is the trench. The white lines highlight the model midplane.

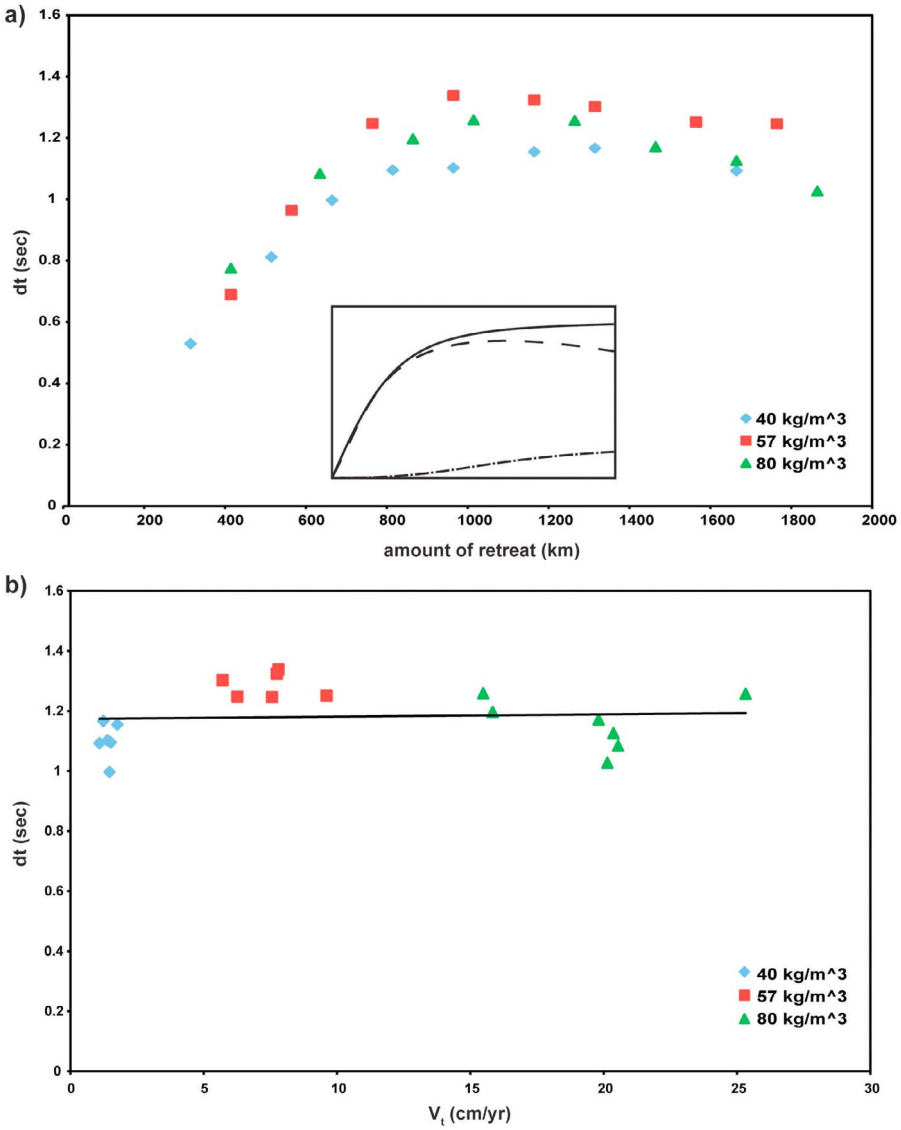

Figure 3. Synthetic SKS subslab δt measurements. Plots of δt versus (a) the amount of retreat and (b) the trench migration velocity. The three sets of points correspond to models with different density contrasts of oceanic plates and fixed trailing edge. Each point is the average of the subslab δt calculated over all seismic stations on the fore-arc. The fore-arc/back-arc transition is assumed to be 200 km from the trench (300 km for the shallow dipping slab with $\Delta\rho = 80$ kg/m^3). Azimuths are aligned $\pm$ 30° from the trench (Figure S5 of Text S1). Seismic stations close to the plate mid-plane are not considered due to the poor coverage of subslab mineral aggregates that tend to diverge from it. The inset in Figure 3a shows inferred trends of the subslab δt versus the amount of retreat with the dashed line the observed pattern. The solid line is δt due to the trench-parallel anisotropy in the lower subslab domain without the destructive interference of δt due to the trench-perpendicular anisotropy forming right beneath the slab (dash-dotted line). In Figure 3b, data shown are those taken after slabs adjust over the 660 km discontinuity (after about 600 km of trench retreat). The black line is the linear fit $\delta t = 0.944 + 0.0083 V_t$ ($R^2 = 0.177$).

core beneath the fore-arc is found, with up to 9% of anisotropy extending laterally over the slab edges following the toroidal flow (Figure 1b). Below the slab toroidal mantle flow is diverging along the plate midplane and is at high angles to the trench-parallel anisotropy (Figure 1d). On the sides of the subduction zone, the fast directions follow the toroidal shear flow around the slab (2–6% anisotropy). Here, the symmetry axes are generally plunging away from the mantle wedge because of the upwelling mantle. The mantle wedge above the slab is characterized by trench-perpendicular fast seismic directions (1–9% anisotropy, Figure 1c), caused by both simple shear and pure shear deformations, associated with the poloidal velocity field and the slab rollback, respectively. Around the subducted tip of the slab laying on the transition zone, strong anisotropy with mostly trench-perpendicular and a downwards plunging symmetry axis develops in response to the strong velocity gradient between the fixed slab tip, lying at the 660 km discontinuity, and the upwelling mantle material, that is carried into the mantle wedge (5–9% anisotropy). Anisotropy in the slab is not considered in our workflow [e.g., *Faccenda et al.*, 2008].

[7] The anisotropic structure of the mantle forms a base for the calculation of SKS splitting as measured at subduction zones. The routines included in the FSTRACK package [*Becker et al.*, 2006] were used to measure synthetic SKS splitting patterns for the model in Figures 1 and S2. The fast shear wave component is mainly trench-parallel in the fore-arc and has delay of $\delta t < 1$ s, whereas it is perpendicular in the back-arc where delays are as high as δt = 1–3 s (Figure 2). The relatively low delay times measured in the fore-arc are due to the disruptive interference among layers with differently oriented symmetry axes. In fact, below the slab the effect of the trench-parallel anisotropy of the lower layer is counteracted by the trench-perpendicular anisotropy in the approximately 100 km thick portion of mantle lying directly beneath the slab. The strength of the upper layer anistropy increases progressively with subduction, especially in the final stages of the model where subduction occurs through plate advance. Because SKS waves are more sensitive to the anisotropy in the shallowest layers [*Schulte-Pelkum and Blackman*, 2003], small trench-parallel seismic anisotropy is then recorded at the surface. On the other hand, in the back-arc the azimuths of the symmetry axes are mostly oriented trench-perpendicular, producing constructive interference among different layers with mostly sub-horizontal symmetry axes that results in large delay times. Delay times decrease toward the plate midplane because the olivine-enstatite aggregates with strong trench parallel anisotropy are squeezed out from this area as a result of the trench-parallel pure shear extension (Figure 1b). On the slab sides, the teleseismic fast shear wave component traces the toroidal flow around the slab edges (δt = 1–2 s), similar to observations in Cascadia, Calabria and possibly the Alaskan arcs [*Civello and Margheriti*, 2004; *Zandt and Humphreys*, 2008; *Christensen and Abers*, 2010].

[8] A further set of models with different density contrast between the oceanic plate and the upper mantle was run, resulting in different velocities, with the aim of understand the relation between the subduction rate and the anisotropy of equally evolving subduction systems. To isolate the effect of plate retreat from the final advancing phase, the plates are blocked at the rear so that they can only retreat. Such models resemble the dynamic of the Calabrian and South Sandwich subduction systems where the relatively narrow slab is attached to a much larger, non-subducting plate, maximizing retreat motions.

[9] In models where subduction occurs at largely different rates, the distribution and amount of seismic anisotropy and SKS splitting are mostly the same (Figure S4 of Text S1). The subslab SKS azimuths are oriented sub-parallel to the trench in the forearc (Figure S5 of Text S1). The subslab δt increases rapidly until the trench has retreated about 1000–1200 km, with the trench-parallel anisotropy approaching its maximum magnitude (Figure S6 of Text S1). The progressive growth of the trench-perpendicular anisotropy beneath the slab interferes destructively with the deeper trench-parallel anisotropy, such that δt measured at the models' surface decreases (Figure 3a). Nevertheless, delay times are considerably higher than those in the dynamic model of Figures 1 and S2, because there is no plate advancing with little trench-perpendicular anisotropy forming below the slab (Figure S4c of Text S1). This comparison illustrates that slab retreat favors trench-parallel anisotropy, while plate advance enhances trench-perpendicular anisotropy.

[10] There is no clear relationship between δt and the trench migration velocity (Figure 3b), showing that seismic anisotropy depends only on the amount of subduction and not on the rate at which the trench migrates (i.e., retreating/advancing).

4. Discussion and Conclusions

[11] A robust feature of the models is a strongly anisotropic core below the fore-arc, yielding subslab delay times of 0.5 to 1.3 sec and trench-parallel azimuths. The subslab anisotropy source in our models matches the location of the anisotropy on Earth [*Müller et al.*, 2008; *Foley and Long*, 2011; *Di Leo et al.*, 2012] and the consistent splitting trench-parallel azimuths reproduce what is a general characteristic of natural subduction zones. Although our synthetic delay times are comparable with δt measured at most subduction zones, few convergent margins have average δt larger by 10 to 30%, namely Calabria and Tonga [*Long and Becker*, 2010], that our models cannot reproduce.

[12] This discrepancy might be reduced when the destructive interference between the upper and lower subslab layers is diminished. Thermal and mechanical (i.e., grain-size dependent) rheological weakening feedbacks not considered here act to thin the layer beneath the slab. This would decrease the effect of the trench-perpendicular anisotropy in favor of the trench-parallel anisotropy that, as a result, might increase the δt to the value reported. Alternatively, fault-induced seismic anisotropy by hydration in subducting oceanic plates might interfere constructively with the trench-parallel subslab mantle anisotropy [*Faccenda et al.*, 2008], yielding higher delay times. It is worth to note that other complexities may arise when water is present in the mantle [e.g., *Jung and Karato*, 2001]. However, this case should be more relevant to the mantle wedge where significant amount of water is released during slab dehydration.

[13] Models where the oceanic plate retreats at different rates indicate that the strength of trench-parallel anisotropy depends only on the amount of retreat and not at which rate the trench migrates (Figures 3, S4, and S5). This is consistent with the basic understanding of petrophysics according to which the LPO is a function exclusively of finite strain and not of strain rate [*Ribe*, 1992; *Zhang and Karato*, 1995; *Bystricky et al.*, 2000].

[14] Although we cannot rule out the occurrence of trench parallel mantle flow that may establish in response to along-trench pressure gradients [*Russo and Silver*, 1994; *Long and Silver*, 2008], our results suggest that it is not needed to reconcile the splitting patterns with the anisotropy at depth, with the condition that slab retreat dominates over slab advance.

[15] **Acknowledgments.** This work has been supported by grants DP0987374 and DP110101697 to F.A.C.; Edouard Kaminski, Thorsten Becker and Vera Schulte-Pelkum are acknowledged for clarifications and discussion about D-Rex and SKS splitting modeling. This paper has been improved by the constructive review of Edouard Kaminski and an anonymous reviewer. Rebecca Farrington improved the paper.

[16] The Editor thanks Edouard Kaminski and an anonymous reviewer for assisting in the evaluation of this paper.

References

Becker, T. W., V. Schulte-Pelkum, D. K. Blackman, J. B. Kellogg, and R. J. O'Connell (2006), Mantle flow under the western United States

from shear wave splitting, *Earth Planet. Sci. Lett.*, *247*, 235–251, doi:10.1016/j.epsl.2006.05.010.

Buttles, J., and P. Olson (1998), A laboratory model of subduction zone anisotropy, *Earth Planet. Sci. Lett.*, *164*, 245–262, doi:10.1016/S0012-821X(98)00211-8.

Bystricky, M., K. Kunze, L. Burlini, and J.-P. Burg (2000), High shear strain of olivine aggregates: Rheological and seismic consequences, *Science*, *290*, 1564–1567, doi:10.1126/science.290.5496.1564.

Christensen, D. H., and G. A. Abers (2010), Seismic anisotropy under Alaska from SKS splitting observations, *J. Geophys. Res.*, *115*, B04315, doi:10.1029/2009JB006712.

Civello, S., and L. Margheriti (2004), Toroidal mantle flow around the Calabrian slab (Italy) from SKS splitting, *Geophys. Res. Lett.*, *31*, L10601, doi:10.1029/2004GL019607.

Di Leo, J. F., et al. (2012), Deformation and mantle flow beneath the Sangihe subduction zone from seismic anisotropy, *Phys. Earth Planet. Inter.*, *194–195*, 38–54, doi:10.1016/j.pepi.2012.01.008.

Faccenda, M., T. V. Gerya, L. Burlini, and D. Mainprice (2008), Fault-induced seismic anisotropy by hydration in subducting oceanic plates, *Nature*, *455*, 1097–1100, doi:10.1038/nature07376.

Foley, B. J., and M. D. Long (2011), Upper and mid-mantle anisotropy beneath the Tonga slab, *Geophys. Res. Lett.*, *38*, L02303, doi:10.1029/2010GL046021.

Funiciello, F., M. Moroni, C. Piromallo, C. Faccenna, A. Cenedese, and H. A. Bui (2006), Mapping mantle flow during retreating subduction: Laboratory models analyzed by feature tracking, *J. Geophys. Res.*, *111*, B03402, doi:10.1029/2005JB003792.

Jung, H., and S. Karato (2001), Water-induced fabric transition in olivine, *Science*, *293*, 1460–1463, doi:10.1126/science.1062235.

Kaminski, E., and N. M. Ribe (2002), Timescales for the evolution of seismic anisotropy in mantle flow, *Geochem. Geophys. Geosyst.*, *3*(8), 1051, doi:10.1029/2001GC000222.

Kaminski, E., N. M. Ribe, and T. Browaeys (2004), D-Rex, a program for calculation of seismic anisotropy due to crystal lattice preferred orientation in the convective upper mantle, *Geophys. J. Int.*, *158*, 744–752, doi:10.1111/j.1365-246X.2004.02308.x.

Karato, S., S. Zhang, and H. Wenk (1995), Superplasticity in the Earth's lower mantle: Evidence from seismic anisotropy and rock physics, *Science*, *270*, 458–461, doi:10.1126/science.270.5235.458.

Kincaid, C., and R. W. Griffiths (2003), Laboratory models of the thermal evolution of the mantle during rollback subduction, *Nature*, *425*, 58–62, doi:10.1038/nature01923.

Long, M. D., and T. W. Becker (2010), Mantle dynamics and seismic anisotropy, *Earth Planet. Sci. Lett.*, *297*, 341–354, doi:10.1016/j.epsl.2010.06.036.

Long, M. D., and P. Silver (2008), The subduction zone flow field from seismic anisotropy: A global view, *Science*, *319*, 315, doi:10.1126/science.1150809.

McKenzie, D. (1979), Finite deformation during fluid flow, *Geophys. J. R. Astron. Soc.*, *58*, 689–715, doi:10.1111/j.1365-246X.1979.tb04803.x.

Moresi, L., et al. (2007), Computational approaches to studying non-linear dynamics of the crust and mantle, *Phys. Earth Planet. Inter.*, *163*, 69–82, doi:10.1016/j.pepi.2007.06.009.

Müller, C., B. Bayer, A. Eckstaller, and H. Miller (2008), Mantle flow in the South Sandwich subduction environment from source-side shear wave splitting, *Geophys. Res. Lett.*, *35*, L03301, doi:10.1029/2007GL032411.

Park, J., and V. Levin (2002), Seismic anisotropy: Tracing plate dynamics in the mantle, *Science*, *296*, 485–489, doi:10.1126/science.1067319.

Piromallo, C., T. W. Becker, F. Funiciello, and C. Faccenna (2006), Three-dimensional instantaneous flow induced by subduction, *Geophys. Res. Lett.*, *33*, L08304, doi:10.1029/2005GL025390.

Ribe, N. M. (1992), On the relation between seismic anisotropy and finite strain, *J. Geophys. Res.*, *97*, 8737–8747, doi:10.1029/92JB00551.

Russo, R. M., and P. G. Silver (1994), Trench-parallel flow beneath the Nazca plate from seismic anisotropy, *Science*, *263*, 1105–1111, doi:10.1126/science.263.5150.1105.

Savage, M. K. (1999), Seismic anisotropy and mantle deformation: What have we learned from shear wave splitting?, *Rev. Geophys.*, *37*, 65–106, doi:10.1029/98RG02075.

Schulte-Pelkum, V., and D. K. Blackman (2003), A synthesis of seismic P and S anisotropy, *Geophys. J. Int.*, *154*, 166–178, doi:10.1046/j.1365-246X.2003.01951.x.

Tommasi, A., D. Mainprice, P. Cordier, C. Thoraval, and H. Couvy (2004), Strain-induced seismic anisotropy of wadsleyite polycrystals and flow patterns in the mantle transition zone, *J. Geophys. Res.*, *109*, B12405, doi:10.1029/2004JB003158.

Zandt, G., and E. D. Humphreys (2008), Toroidal mantle flow through the western U.S. slab window, *Geology*, *36*, 295–298, doi:10.1130/G24611A.1.

Zhang, S., and S. Karato (1995), Lattice preferred orientation of olivine aggregates deformed in simple shear, *Nature*, *375*, 774–777, doi:10.1038/375774a0.